Moderate downregulation of NDUFA13 promotes cardiomyocytes proliferation and heart regeneration through the glycolysis/c-Myc/*Ccnd1* axis

YING GAO[1-3*], NINGJING QIAN[1-3*], JUNYAN JIN[1-3], JIAYI LIU[1-3], BINGQI WANG[1-3] and YAPING WANG[1-3]

[1]Department of Cardiology, The Second Affiliated Hospital, School of Medicine, Zhejiang University, Hangzhou, Zhejiang 310009, P.R. China; [2]State Key Laboratory of Transvascular Implantation Devices, Hangzhou, Zhejiang 310009, P.R. China; [3]Heart Regeneration and Repair Key Laboratory of Zhejiang Province, Hangzhou, Zhejiang 310009, P.R. China

Received October 1, 2025; Accepted March 4, 2026

DOI: 10.3892/ijmm.2026.5890

Abstract. The poor prognosis of heart diseases is largely attributable to the limited proliferative capacity of cardiomyocytes. Cardiomyocyte proliferation and heart regeneration has garnered increasing attention, with a focus on the identification of novel therapeutic targets. In the present study, NADH dehydrogenase ubiquinone I α subcomplex 13 (NDUFA13), a subunit protein of mitochondria complex I, was found to serve an important role during this regenerative period of cardiomyocytes. Both *in vitro* and *in vivo*, moderate downregulation of NDUFA13 promoted cardiomyocytes proliferation, increased expression of cell cycle genes, reduced fibrosis and thus benefitted heart regeneration after apical resection. In addition, downregulation of NDUFA13 not only preserved mitochondrial function but also enhanced glycolysis, which is a metabolic shift that is important for modulating the state of cardiomyocytes. Using western blot and reverse transcription-quantitative PCR, NDUFA13 expression was analyzed at different growth stages in mice and identified its association with cardiomyocyte proliferation. To investigate the role of NDUFA13 *in vitro*, a moderately NDUFA13-downregulated cell model was developed using siRNA; *in vivo*, *Myh6*-cre^{ERT} *Ndufa13*$^{flox/+}$ mice were generated and performed apical resection surgery. Through proliferation markers, echocardiography and fibrotic staining, the relationship between NDUFA13 and heart regeneration was revealed. To investigate the functional mechanisms, oxidative phosphorylation and glycolytic activity in NDUFA13-downregulated primary cardiomyocytes was assessed. Upon confirming the changes in glycolytic flux, the expression of c-Myc and key cell cycle-related genes was measured. Chromatin immunoprecipitation experiments further revealed c-Myc binding to the promoter region of *Ccnd1*. Increasing levels of glycolysis upregulated the expression of c-Myc, which could bind to the promotor zone of cell cycle gene cyclin D1, thus promoting cardiomyocytes proliferation. Through mitochondrial-nuclear communication, signals originating from the mitochondria are converted into nuclear transcriptional responses, which in turn drive cellular proliferation. Therefore, the present study demonstrated the key role of NDUFA13 in cardiac regeneration and its potential as a target for heart injury treatment.

Correspondence to: Dr Yaping Wang, Department of Cardiology, The Second Affiliated Hospital, School of Medicine, Zhejiang University, 88 Jiefang Road, Hangzhou, Zhejiang 310009, P.R. China
E-mail: yapingwang@zju.edu.cn

*Contributed equally

Abbreviations: NDUFA13, NADH dehydrogenase ubiquinone I α subcomplex 13; c-Myc, cellular myelocytomatosis oncogene; Ccnd1, cyclin D1; NMCMs, neonatal mouse cardiomyocytes; Pfkfb3, 6-phosphofructo-2-kinase/fructose-2,6-bisphosphatase 3; Hk2, hexokinase 2; Pkm2, pyruvate kinase muscle isozyme M2; Sdha, succinate dehydrogenase complex flavoprotein subunit A; Cox15, cytochrome c oxidase assembly homolog 15; Ccne1, cyclin E1; Cdc20, cell division cycle 20

Key words: NDUFA13, cardiomyocyte proliferation, heart regeneration, glycolysis, c-Myc

Introduction

With an increasing prevalence in aging populations, the incidence and prevalence of cardiovascular diseases (CVDs) are increasing rapidly (1,2). CVDs accounted for 437 million disability-adjusted life years and 19.2 million associated mortalities worldwide in 2023 (3). The limited regenerative capacity of adult cardiomyocytes, which fail to proliferate in response to injuries such as ischemia or mechanical stress, is a key factor underlying the poor prognosis of numerous heart conditions (4,5). At present, for various heart diseases, the main treatments include conventional drug therapy, interventional therapy and heart transplantation (6,7). However, poor efficacy and high cost of the present strategies remain considerable barriers that need to be solved urgently.

Cardiomyocytes have long been considered terminally differentiated cells with no capacity for renewal. However, in 2002, Poss *et al* (8) removed ~20 percent of the ventricle from a zebrafish, finding for the first time that its heart could

regenerate completely without scarring. This finding was extended to mammals when Porrello *et al* (9) observed a similar, albeit transient, regenerative ability in neonatal mice. However, this recovery capacity decreases gradually with age. Within the 7 days after birth, the regenerative ability of the heart declines considerably, and thereafter complete scar-free regeneration becomes virtually unachievable. In adult human hearts, the rate of proliferation of cardiomyocytes is normally 0.3-1.0% per year, and this proportion increases slightly under pathological conditions (10-12). Therefore, the present study aimed to identify novel targets of cardiomyocyte proliferation, to provide new strategies for treatment of cardiovascular diseases.

NADH dehydrogenase ubiquinone I α subcomplex 13 (NDUFA13), as known as GRIM-19, is a subunit of mitochondrial complex I, which was discovered during the usage of interferon combined with retinoic acid to induce apoptosis (12). NDUFA13 expression is significantly reduced in numerous types of tumors, such as hepatocellular carcinoma and breast carcinoma (13-15) and was initially regarded as one of the key targets for regulating tumor cell growth (16). Further evidence indicates that NDUFA13 not only serves a role in electron transport and maintenance of membrane potential homeostasis in mitochondria, but also affects the regulation of cell cycle and supports cell movement (17,18). Given that, NDUFA13 plays important roles in energy metabolism and cell proliferation, which are both crucial to cardiomyocyte proliferation, we hypothesize that NDUFA13 may play a regulatory role in cardiomyocyte proliferation. Therefore, the present study sought to explore whether NDUFA13 can regulate the cardiomyocytes proliferation and myocardial regeneration in response to injury.

Previous studies have reported that neonatal cardiomyocytes utilize glycolysis as the main form of metabolism (19-21), and which will gradually transit to oxidative phosphorylation and fatty acid metabolism in adulthood, accompanied by the loss of cardiomyocyte proliferative capacity. It has been suggested that increasing the levels of glycolysis can promote cardiomyocytes to re-enter the cell cycle (22). Previous work by Li *et al* (23) showed that knock out of the key enzyme gene *Cpt1b* triggers a metabolic shift, results in α-ketoglutarate accumulation. This metabolite activates the histone demethylase lysine demethylase 5B, driving cardiomyocyte dedifferentiation, cell cycle re-entry and ultimately cardiac regeneration. The present study investigated whether the effects of NDUFA13 downregulation are associated with metabolic reprogramming.

Materials and methods

Animals and mice apical resection model. All wild type C57BL/6J mice (age, 6-8 weeks; weight, 20-25 g) were obtained from Shanghai Laboratory Animal Research Center. Mice with *Ndufa13* loxP sites and *Myh6*-Cre^{ERtam} mice were generated and obtained from the Shanghai Biomodel Organisms Center. All mice were maintained at the Laboratory Animal Center, Hangzhou Medical College (Hangzhou, China) (all animal experiments and housing procedures were conducted under a legally signed cooperation agreement between our institution and Hangzhou Academy of Medical Sciences). The animals were housed under specific pathogen-free conditions, with moderate temperature and humidity, and 12 h light-dark circle. A temperature of 22-25˚C and a relative humidity of 40-60% were controlled. The mice had easy access to standard chow and filtered water throughout the experiment.

The present study was approved by The Animal Ethics Committee of The Second Affiliated Hospital, Zhejiang University School of Medicine (Hangzhou, China; approval no. 2019-NO.033). All experimental procedures were performed according to institutional guidelines and the Guide for the Care and Use of Laboratory Animals (24-26). Humane endpoints were strictly observed to minimize animal suffering. Animals were humanely euthanized if they exhibited any of the following signs: i) Weight loss: A rapid decline of >20% of initial body weight within 48 h or >25% at any point; or ii) physical condition: Signs of severe pain/distress, massive hemorrhage, severe wound infection and anorexia.

Tamoxifen injection. Prior to injection, a 1 mg/ml tamoxifen solution was prepared. On the day of birth, the hand used to handle the mice was rubbed in the bedding, and a suckling mouse pup was removed and held head-down in hand to reveal the stomach. The tip of a 30G needle was used to puncture the stomach to gradually inject 50 μl of tamoxifen solution, following which the needle tip was slowly removed. The injection was repeated on the 2nd and 3rd day after birth.

Apical resection model. Neonatal mice were anesthetized over ice, with a paper towel layer that prevented direct contact; a state of anesthesia was achieved when the skin of the mice turned gray. The mice were fixed on the operating table in a supine position. Following disinfection, a 0.5-1.0 cm surgical incision was made transversely in the fourth intercostal space using micro-scissors. Microscopic forceps were used for blunt separation of the intercostal muscles to expose the surgical field. The pressure on the abdomen was slightly manually increased so that the apex of the heart was exposed from the incision site. The apical portion was cut off using micro-scissors, which occupied ~10% of the total ventricle. Following this, 8-0 surgical sutures were used to suture the intercostal space, ensuring the intercostal space was fully closed and 11-0 threads were used to suture the skin, hiding as much of the thread in the skin as possible. The entire surgical procedure was completed within 10 min. After surgery, mice were placed under a warm light to rewarm gradually. When the skin of the mice turned from gray to red, the urine of the maternal mouse was collected and coated onto the skin of the neonatal mice and the neonatal mice were returned to their cage.

A total of 30 mice in the control (Myh6-cre^{ERT}:Ndufa13$^{+/+}$ mice) and *Ndufa13*$^{+/-}$ groups that underwent apical resection were assessed for relevant indicators at postoperative day 3 (control, n=6; *Ndufa13*$^{+/-}$, n=8), day 7 (n=4 each) and day 21 (n=4 each). A total of 35 surgical procedures were performed, with 5 perioperative mortalities recorded, primarily due to massive hemorrhage.

Heart isolation process. Pregnant mice (on embryonic day 15.5, E15.5) and adult mice were anesthetized via inhalation of 3% isoflurane, and anesthesia maintained using 1% isoflurane. For E15.5 embryos, following anesthesia of the pregnant dam, its abdominal cavity was opened and the uterine horn was excised. After rinsing with phosphate-buffered

saline (PBS), the embryos were dissected free from the embryonic membranes. The heart of each embryo was then carefully isolated under a stereomicroscope. Neonatal mice at postnatal days 0, 3 and 7 were anesthetized on ice, following which the thoracic cavity was opened and the heart was excised by cutting at the aortic root and rinsed in PBS. For adult mice, after anesthesia, the thoracic cavity was opened and the right atrium was incised. PBS was perfused through the left ventricle using a syringe to clear the blood. Following perfusion, the heart was excised by cutting at the aortic root. Mice death was verified by a cessation of respiration and heartbeat.

Echocardiography. Transthoracic echocardiography [VINNO 6 lab; VINNO Technology (Suzhou) Co., Ltd.] was performed at day 21 following apical resection. After isoflurane inhalation anesthetization (induction, 3%; maintenance, 1%), two-dimensional parasternal long axis and short axis view at papillary muscle level were obtained and M-mode images captured to analyze the cardiac structure and function. The heart rate of the mice was maintained at ~500 beats per minute, and their body temperature was kept at 37˚C.

Neonatal mouse cardiomyocytes (NMCMs) isolation and culture. NMCMs were isolated from 1-day-old C57BL/6 mice using the Neonatal Heart Dissociation Kit (cat. no. 130-098-373; Miltenyi Biotec GmbH) as per the manufacturers' instructions. In brief, after hypothermic anesthesia on ice, the chest cavity of the neonatal mice was opened by cutting the fourth intercostal space and the heart was exposed by applying abdominal pressure. The ventricular myocardium from neonatal mice was collected and cut into 1 mm^3 pieces, to which digestive enzymes were mixed and added; digestion was performed three times for 10 min each in total. The digestive enzyme solution was neutralized with DMEM containing 10% fetal bovine serum [Heyuan Liji (Shanghai) Biotechnology Co., Ltd.] and filtered through a 70-μm filter. Following a 15 min adhesion period, the cell suspension was collected. Then, cardiomyocytes were cultured with DMEM (4.5 g/l D-Glucose; Gibco; Thermo Fisher Scientific, Inc.) containing 10% FBS and 1% penicillin and streptomycin (Wuhan Servicebio Technology Co., Ltd.). Cardiomyocytes were incubated at 37˚C in incubator with 5% CO_2.

Isolation of mitochondria from cultured cells. Mitochondria was isolated from cultured cells using the Mitochondrial Isolation and Protein Extraction kit (cat. no. PK10016; Proteintech Group, Inc.), according to the manufacturers' instruction. Briefly, the cells were harvested and centrifuged at 500 x g for 5 min at 4˚C. The pellet was washed twice with ice-cold PBS. On ice, 1 ml of ice-cold mitochondrial isolation reagent A for every 20 million cells was added directly to the pellet. The suspension was then transferred to a pre-chilled glass homogenizer for 3-5 strokes, and an equal volume of ice-cold mitochondrial isolation reagent B was added to the bottom of a centrifuge tube. The homogenate was then carefully layered on top by slowly pipetting along the tube wall followed by centrifugation and the uppermost layer was collected. A subsequent centrifugation (4˚C; 10,000 x g; 10 min) step separated the crude mitochondria (pellet) from the mitochondria-free cytosolic fraction (supernatant). To prepare high purity mitochondria, high-purity separation medium was used. The crude mitochondrial pellet was resuspended in 0.5 ml (per tube) of mitochondrial wash buffer. The resuspended crude mitochondria were layered on top of the pre-aliquoted high-purity separation medium, and centrifuged at 22,000 x g for 10 min at 4˚C. The final pellet was collected and washed, which contained high-purity mitochondria.

Western blotting. Proteins were extracted from cells or myocardial tissue with RIPA buffer (Beyotime Biotechnology) containing 1X protease and phosphatase inhibitor (Beyotime Biotechnology). The concentration of protein was detected with BCA protein quantification kit (Beyotime Biotechnology). Subsequently, 20-30 μg total protein was added and separated on 10 or 12% SDS-polyacrylamide gels by electrophoresis. Then proteins were transferred onto PVDF membranes (0.22 μm; MilliporeSigma). After 1-2 h blocking (5% non-fat milk; room temperature), immunoblots were incubated with the following primary antibodies overnight at 4˚C: Anti-GRIM19 (1:1,500; cat. no. 10986-1-AP; Proteintech Group, Inc.), anti-c-Myc (1:1,000; cat. no. RT1149; HUABIO), anti-TOMM20 (1:10,000; cat. no. 11802-1-AP; Proteintech Group, Inc.), anti-LDH (1:10,000; cat. no. 14824-1-AP; Proteintech Group, Inc.), anti-Lamin B (1:10,000; cat. no. 12987-1-AP; Proteintech Group, Inc.) and anti-β-tubulin (1:1,000; cat. no. EM1701-59; HUABIO). Membranes were then incubated with horseradish peroxidase-conjugated secondary antibodies 1-2 h at room temperature [multi-rAb® HRP-goat anti-rabbit recombinant secondary antibody (H+L) (cat. no. RGAR001; 1:10,000; Proteintech Group, Inc.) and multi-rAb® HRP-goat anti-mouse recombinant secondary antibody (H+L) (cat. no. RGAM001; 1:10,000; Proteintech Group, Inc.]. The final membranes were visualized ECL chemiluminescent detection reagent (Fdbio Science). The washing buffer used throughout the experiment was PBST containing 0.1% v/v Tween-20. The images were analyzed using the ImageJ software-Fiji (stable) (National Institutes of Health).

Reverse transcription-quantitative polymerase chain reaction. Total RNA was extracted from cell and myocardium using RNA isolater total RNA extraction reagent (Vazyme Biotech Co., Ltd.) and quantified with NanoDrop One spectrophotometer (Thermo Fisher Scientific, Inc.) Total RNA was reverse-transcribed into cDNA using the reverse transcription kit (Accurate Biology). qPCR was performed using the SYBR Green Master Mix (TransGen Biotech Co., Ltd.) with a LightCycler 480 II (Roche Diagnostics). The procedure was as follows: Initial denaturation at 95˚C for 5 min, followed by 40 cycles of denaturation at 95˚C for 10 sec and combined annealing/extension at 60˚C for 30 sec, with a final extension at 72˚C for 5 min. Gene expression was calculated via the $2^{-\Delta\Delta Cq}$ method (27), using the internal gene *Actb* and control group as reference values. qPCR primer sequences are shown in Table I.

Immunofluorescent and immunohistochemistry staining. For hearts tissues (different stages of hearts and hearts collected at 21 days after apical resection), following tissue collection, specimens were fixed in 4% paraformaldehyde (PFA) for 24 h at room temperature prior to embedding

Table I. Quantitative PCR primers.

Gene	Direction	Sequence (5'-3')
Ndufa13	Forward	AGGTGGGCGAGTCTGTGTTCC
	Reverse	GGCATTGCTCATCTCCTCCTTGG
Ccnb1	Forward	CTTGAACATGTTAGAGAAGAGAAGC
	Reverse	TCGGGCTTGGAGAGGGATTA
Ccnd1	Forward	CGTATCTTACTTCAAGTGCGTG
	Reverse	ATGGTCTCCTTCATCTTAGAGG
Ccne1	Forward	GCACCAGTTTGCTTATGTTACA
	Reverse	GGGCCTTCATCATCATCAATTC
Cdc20	Forward	AACAGGAGGAGGAACCAGTGACC
	Reverse	GCACATCCACAGCACTCAGACAG
Pcna	Forward	GAAGTTTTCTGCAAGTGGAGAG
	Reverse	CAGGCTCATTCATCTCTATGGT
Cdk4	Forward	GAGTGTGAGAGTTCCTAATGGA
	Reverse	GGTCCTGGTCTATATGCTCAAA
Pfkfb3	Forward	TCATCGAGTCGGTCTGTGACGA
	Reverse	CATGGCTTCTGCTGAGTTGCAG
Hk2	Forward	CCCTGTGAAGATGTTGCCCACT
	Reverse	CCTTCGCTTGCCATTACGCACG
Pkm2	Forward	CAGAGAAGGTCTTCCTGGCTCA
	Reverse	GCCACATCACTGCCTTCAGCAC
Sdha	Forward	GAGATACGCACCTGTTGCCAAG
	Reverse	GGTAGACGTGATCTTTCTCAGGG
Cox15	Forward	GGTCAGCACTGGTTCTCTACTG
	Reverse	CAGCAAACCGTCTCAACCACAG
Atp5f1a	Forward	GCCCTCGGTAATGCTATTGA
	Reverse	GCAATCGATGTTTTCCCAGT
Actb	Forward	CATTGCTGACAGGATGCAGAAGG
	Reverse	TGCTGGAAGGTGGACAGTGAGG

NDUFA13, NADH dehydrogenase ubiquinone I α subcomplex 13; Ccnb1, Cyclin B1; Ccnd1, cyclin D1; Pfkfb3, 6-phosphofructo-2-kinase/fructose-2,6-bisphosphatase 3; Hk2, hexokinase 2; Pkm2, pyruvate kinase muscle isozyme M2; Sdha, succinate dehydrogenase complex flavoprotein subunit A; Cox15, cytochrome c oxidase assembly homolog 15; Cdc20, cell division cycle 20; F, forward; R, reverse.

in paraffin wax and sectioning at a thickness of 4 μm for further use. Prior to staining, sections were deparaffinized in xylene and rehydrated through a graded ethanol series (100, 95 and 70%). Heat-induced epitope retrieval was performed by heating sections in citrate buffer (pH 6.0) to 95-125˚C for 10-20 min.

For the frozen sections (hearts collected at 3, 7 days after apical resection), specimens were dehydrated in 30% sucrose solution at 4˚C overnight, embedded in optimal cutting temperature compound (Sakura Finetek Europe B.V.), snap-frozen in isopentane cooled with liquid nitrogen, and stored at -80˚C until sectioning. Frozen sections were cut at a thickness of 7 μm and fixed in 4% PFA for 20 min for further immunofluorescent staining. For both immunofluorescent and immunohistochemical staining, the samples were then permeabilized using 0.3% Triton X-100 for 15 min and blocked with 5% bovine serum albumin for 1 h, the samples were incubated with primary antibodies overnight at 4˚C using the following: Anti-GRIM19 (1:500; cat. no. 10986-1-AP; Proteintech Group, Inc.), Ki67 (1:500; cat. no. ab16667; Abcam), aurora B (1:800; cat. no. ab2254; Abcam), phosphohistone H3 (pH3; 1:500; cat. no. 06-570; Sigma-Adrich; Merck KGaA), cardiac troponin I (cTnI; 1:800; cat. no. 66376; Proteintech Group, Inc.). For immunofluorescent staining, the slides were washed three times in PBS and incubated with the corresponding second antibody: Goat anti-rabbit IgG H&L (Alexa Fluor® 488) (1:400; cat. no. ab150165; Abcam), goat anti-mouse IgG H&L (Alexa Fluor® 488) (1:400; cat. no. A-1100; Invitrogen; Thermo Fisher Scientific, Inc.), donkey anti-rabbit IgG (H&L) DyLight™ 550 (1:400; cat. no. ab96892; Abcam) and donkey anti-mouse IgG (H&L) DyLight™ 550 (1:400; cat. no. ab96876; Abcam). Finally, the slices were incubated with DAPI (cat. no. G1012; Wuhan Servicebio Technology Co., Ltd.) and covered with antifade mounting medium.

For immunohistochemistry staining, following primary antibody incubation, the slices were washed and incubated with second antibody (cat. no. PV6001; ZSGB-BIO) for 1 h at room temperature. Slices were then stained with DAB staining

solution (cat. no. PV6001; ZSGB-BIO). Images were acquired using a fluorescent microscope (Leica Biosystems) and quantified using the ImageJ software-Fiji.

Cells were fixed with 4% PFA for 15 min and then incubated in 0.3% Triton X-100 for 15 min at room temperature. After blocking with 5% bovine serum albumin for 1 h, cells were incubated with primary antibodies overnight at 4˚C: cTnI (1:800; cat. no. 66376; Proteintech Group, Inc.) and vimentin (1:100; cat. no. 5741; CST Biological Reagents Co., Ltd.). Cells were washed three times in PBS and incubated with the corresponding secondary antibody for 1 h at room temperature: Goat anti-mouse IgG (H&L) Alexa Fluor® 488 (1:400; cat. no. ab150113; Abcam) and donkey anti-rabbit IgG (H&L) DyLight™ 550 (1:400; cat. no. ab96892; Abcam). Finally, the cells were incubated with DAPI for 15 min at room temperature (cat. no. G1012; Wuhan Servicebio Technology Co., Ltd.) and covered with anti-fade mounting medium (Fig. S1) (28,29). Images were acquired using a fluorescent microscope (Leica Biosystems) and quantified using the ImageJ software-Fiji.

Hematoxylin and eosin (H&E) and Masson's trichrome staining. Paraffin sections at a thickness of 4 μm were used for H&E and Masson's trichrome staining. The slices were dewaxed and washed in PBS as aforementioned. H&E staining were then performed according to standard protocols. Briefly, the sections were immersed in hematoxylin solution for 5-10 min, differentiated in 1% hydrochloric acid ethanol for several seconds, and immediately blued in tap water for 5-10 min (all at room temperature). Eosin solution was used to stain the sections for 30 sec to 1 min at room temperature. Masson's trichrome staining was performed according to the manufacturer's instructions (cat. no. G1346; Beijing Solarbio Science & Technology Co., Ltd.). The images were acquired using a light microscope (Leica Microsystems, Inc.) and quantified using ImageJ software.

Small interfering RNA (siRNA) transfection. Specific siRNAs were obtained from Sangon Biotech Co., Ltd., as follows: SiRNA targeting *Ndufa13,* sense (S), 5'-CCAUCG ACUACAAGCGGAA-3' and anti-sense (AS), 5'-UUCCGC UUGUAGUCGAUGG-3'; and scramble control S, 5'-UUC UCCGAACGUGUCACGU/dT//dT/-3' and AS, 5'-ACG UGACACGUUCGGAGAA/dT//dT/-3'. Both siRNA and scramble RNA were transfected into primary cardiomyocytes with Lipofectamine 3000 (Thermo Fisher Scientific, Inc.) according to the manufacturer's instructions. Briefly, using 12-well plates for example, cells were transfected with 100 nM siRNA in serum-free and antibiotics-free DMEM containing 2.4 μl of Lipofectamine® 3000 (Thermo Fisher Scientific, Inc.) at 37˚C (30). The medium was changed 6 h later to normal complete medium. Cells were harvested 72 h after transfection to measure the expression levels of *Ndufa13*.

CCK-8 assay. Primary cardiomyocytes were seeded into a 96-well cell culture plate at $5x10^3$ cells per well. The outer perimeter wells were filled with 100 μl of sterile PBS to minimize evaporation and edge effects. The plate was then incubated under standard culture conditions (37˚C, 5% CO_2). Following cell attachment, siRNA transfection was performed as aforementioned. At the end of the treatment period, 10 μl of the CCK8 reagent (cat. no. K1018; APexBIO Technology LLC) was added directly to each well containing 100 μl of medium. The plate was gently shaken to ensure thorough mixing. The plate was returned to the incubator (37˚C, 5% CO_2) and incubated for 1-4 h. Following incubation, the absorbance of each well was measured at a wavelength of 450 nm using a microplate reader.

Flow cytometry for cell cycle analysis. Following siRNA treatment, primary cardiomyocytes were harvested by trypsinization, washed twice with cold PBS. Cells were fixed by gentle resuspension in 1 ml of ice-cold 70% ethanol and incubation at 4˚C for a minimum of 2 h or overnight. Fixed cells were pelleted by centrifugation at 300 x g for 5 min at 4˚C and washed once with cold PBS to remove residual ethanol. The cell pellet was resuspended in 500 μl of a staining solution containing propidium iodide (50 μg/ml) and RNase A (100 μg/ml) in PBS. The suspension was incubated in the dark at 37˚C for 30 min. Stained samples were analyzed using a Fortessa X20 flow cytometer (BD Biosciences) and the PE channel served as the detection channel. Data were analyzed through Flowjo VX (BD Biosciences).

Oxygen consumption rate (OCR) and extracellular acidification rate (ECAR). OCR and ECAR tests were performed using the Agilent Seahorse XFe96 Analyzer (Agilent Technologies, Inc.) according to corresponding instructions. For OCR, the order of drug addition was as follows: Oligomycin (1.5 μM), carbonyl cyanide-4-(trifluoromethoxy)phenylhydrazone (FCCP) (1.5 μM), rotenone and antimycin A (0.5 μM each). For ECAR, the order of drug addition was as follows: Glucose (10 mM), oligomycin (1 mM) and 2-deoxy-glucose (50 mM).

Chromatin immunoprecipitation (ChIP). The genomic sequence of cyclin D1 (*Ccnd1*; gene ID 12443) was retrieved from the UCSC database (GRCm39/mm39) (https://genome.ucsc.edu/). The sequence used for following primer design is from chromosome 7: 144,493,368-144,495,568, which contains high-probability functional binding region for promotor. The JASPAR database (https://jaspar.elixir.no/) was used to predict potential binding sites for *Ccnd1* and c-Myc (CCTCGTGCTT). Based on the binding sites, primers were designed for subsequent experimental validation, as follows: Forward primer, 5'-AGGCTAAGGCTCCCAGGCTTG-3' and reverse, 5'-GTG ATTCCACTGTAGCTCCGAAGG-3'. The primer pair amplifies a 97-bp fragment at chr7:144,495,016-144,495,112.

ChIP assays were performed according to the manufacturer's instructions of the BeyoChIP™ Enzymatic ChIP Assay Kit (Protein A/G) (cat. no. P2083S; Beyotime Biotechnology). Briefly, cells were cross-linked with 1% formaldehyde at 37˚C for 10 min, and glycine was added at room temperature for 5 min to stop the cross-linking. After cells were washed in different buffers, chromatin was digested into small fragments (200-1,000 bp) with MNase (2,000 gel units; 37˚C; 20 min). The normal IgG or anti-c-Myc antibody (0.5-2.0 μg; cat. no. HA721182; HUABIO) were added into supernatant (4˚C; 12,000-14,000 x g; 5 min) and incubated overnight at 4˚C to form the target protein-DNA complex. The next day, the IgG/A magnetic beads were added and incubated for 1 h at

4˚C. Then, after washing with low salt immune complex wash buffer, high salt immune complex wash buffer, LiCl immune complex wash buffer and TE buffer, the final complex was extracted. Finally, DNA fragments were purified and analyzed via PCR and qPCR. For PCR, the procedure was: Initial temperature at 94˚C for 3 min, followed by 35 cycles of 94˚C for 30 sec, 58˚C for 30 sec and 72˚C for 1 min, and a final step at 72˚C for 5 min. The PCR products were subjected to electrophoresis on a 1.5% agarose gel for 30 min, and then visualized using the Bio-Rad GelDoc Go system (Bio-Rad Laboratories, Inc.). The qPCR procedure was as described previously.

2-NBDG uptake assay. The 2-NBDG uptake assay was performed according to the manufacturer's instructions of the glucose uptake fluorescence assay kit with 2-NBDG (2-NBDG) (cat. no. S0561S; Beyotime Biotechnology). Briefly, cardiomyocytes were seeded in 96-well black plates at a density of $1x10^4$ cells per well, and cultured in complete medium. After siRNA transfection, the medium was changed to glucose-free medium and incubated at 37˚C for 1 h to induce glucose starvation. Then, 2-NBDG (1:100 with medium) was added and the cells incubated at 37˚C with 5% CO_2 in the dark for 30-60 min. The fluorescence intensity was detected using a multi-functional microplate reader (Excitation wavelength, 488 nm; emission wavelength, 542 nm).

2-Deoxy-D-glucose assay (2-DG). Cardiomyocytes were seeded in 12-well black plates at $1.5x10^5$ per well. After siRNA transfection, different concentrations (0.5 and 5 mM) of 2-DG were added into the wells and incubated for 48 h at 37˚C. The cells after incubation were harvested for protein isolation.

Resident glucose measurements. The resident glucose measurement assay was performed according to the manufacturer's instructions of the glucose assay kit with O-toluidine (cat. no. S0201S; Beyotime Biotechnology). Briefly, cardiomyocytes were seeded in 96-well black plates at a density of $1x10^4$ cells per well, and cultured in complete medium. After siRNA transfection, cells were cultured for 72 h. Subsequently, 20 μl of standard or sample was pipetted into a PCR tube and 170 μl of glucose assay reagent was added to make the final volume 190 μl. After vortex mixing, the sample was centrifuged at 5,000 x g for a few seconds at room temperature to settle the liquid to the bottom of the tube. The tube was heated at 95˚C for 8 min on a PCR instrument, then cooled down to 4˚C. After cooling to 4˚C, the PCR tubes were removed and 180 μl of liquid from each tube was aspirated into a clean 96-well plate. Air bubbles were avoided when transferring the liquid. The absorbance was measured at 630 nm. The glucose concentration in the sample was calculated according to the standard curve.

Database. Expression levels of NDUFA13 in various tissues was collected from The Genotype-Tissue Expression database (https://www.gtexportal.org/home). Expression levels of NDUFA13 and TOMM20 in different embryonic and neonatal period were collected from the database [Gene Expression Omnibus database; accession no. GSE193346 (31); https://cells-test.gi.ucsc.edu/?ds=mouse-dev-heart]. Expression levels of NDUFA13 at day 3, 7 and 21 after MI compared with that of sham mice was collected from the database (Gene Expression Omnibus database; accession nos. GSE243668 and GSE236374) (32,33).

Statistical analysis. All experiments were repeated >3 times. All data were presented as mean ± standard deviation (mean ± SD), and GraphPad Prism (version 8; Dotmatics) was used for data analysis and statistical graphing. For the data that conformed to normal distribution (Shapiro-Wilk test) and with homogeneous variance, unpaired Student's t-test was used for two groups and the one-way ANOVA test was used for ≥3 groups. The post hoc tests used for multiple comparisons was Tukey's test. For data did not conform to the normal distribution or the variance was uneven, the Mann-Whitney test was used for the two groups and the Kruskal-Wallis test was used for ≥3 groups. The post hoc tests used for multiple comparisons was Dunn's test. $P<0.05$ was considered to indicate a statistically significant difference.

Results

NDUFA13 levels expression are decreased in the neonatal period. Previous studies reported low expression levels of NDUFA13 in numerous tumor tissues, such as hepatocellular carcinoma and breast carcinoma (34,35). To assess the expression levels of NDUFA13 in the heart, the GTEx database was searched to compare the expression of NDUFA13 in various tissues. The results showed that the expression levels of NDUFA13 in myocardium was significantly higher increased compared with that of other tissues, such as brain, liver and lung (Fig. 1A). Based on the high levels of cardiac expression, NDUFA13 expression levels were assessed at 3, 7 and 28 days post-myocardial infarction using a public database (Fig. 1B-D). A significant reduction in NDUFA13 expression was demonstrated when compared with that of the Sham groups, which suggested that NDUFA13 may serve a role in cardiac injury. Given the differences in cardiomyocyte proliferation ability in embryonic, neonatal and adult periods, it was considered that the expression levels of NDUFA13 may be concomitant during these stages of growth. Therefore, NDUFA13 expression levels were further assessed in isolated hearts from E15.5 embryos, neonatal day 0, neonatal day 3, neonatal day 7 and adult mice (Fig. 1E). Protein and RNA were isolated for western blot and qPCR analysis, respectively. The expression levels of NDUFA13 gradually increased from E15.5 to postnatal day 7 and significantly increased in adulthood (Fig. 1F-H). Similarly, immunohistochemical staining of cardiac sections from each corresponding period further validated this expression profile (Fig. 1I). NDUFA13 expression progressively increased during heart development, and thus was inversely associated with the declining proliferative capacity of cardiomyocytes. Notably, a sharp rise in NDUFA13 expression levels was observed during the adult stage, when cardiomyocyte proliferation is markedly diminished.

Cardiomyocytes only account for ~40% of the total number of heart cells, while the rest are fibroblasts, endothelial cells and immune cells (36). In order to determine whether NDUFA13 is predominantly expressed in cardiomyocytes or other cell types, GEO database search was performed, and protein and gene expression assessed in isolated cardiomyocytes and

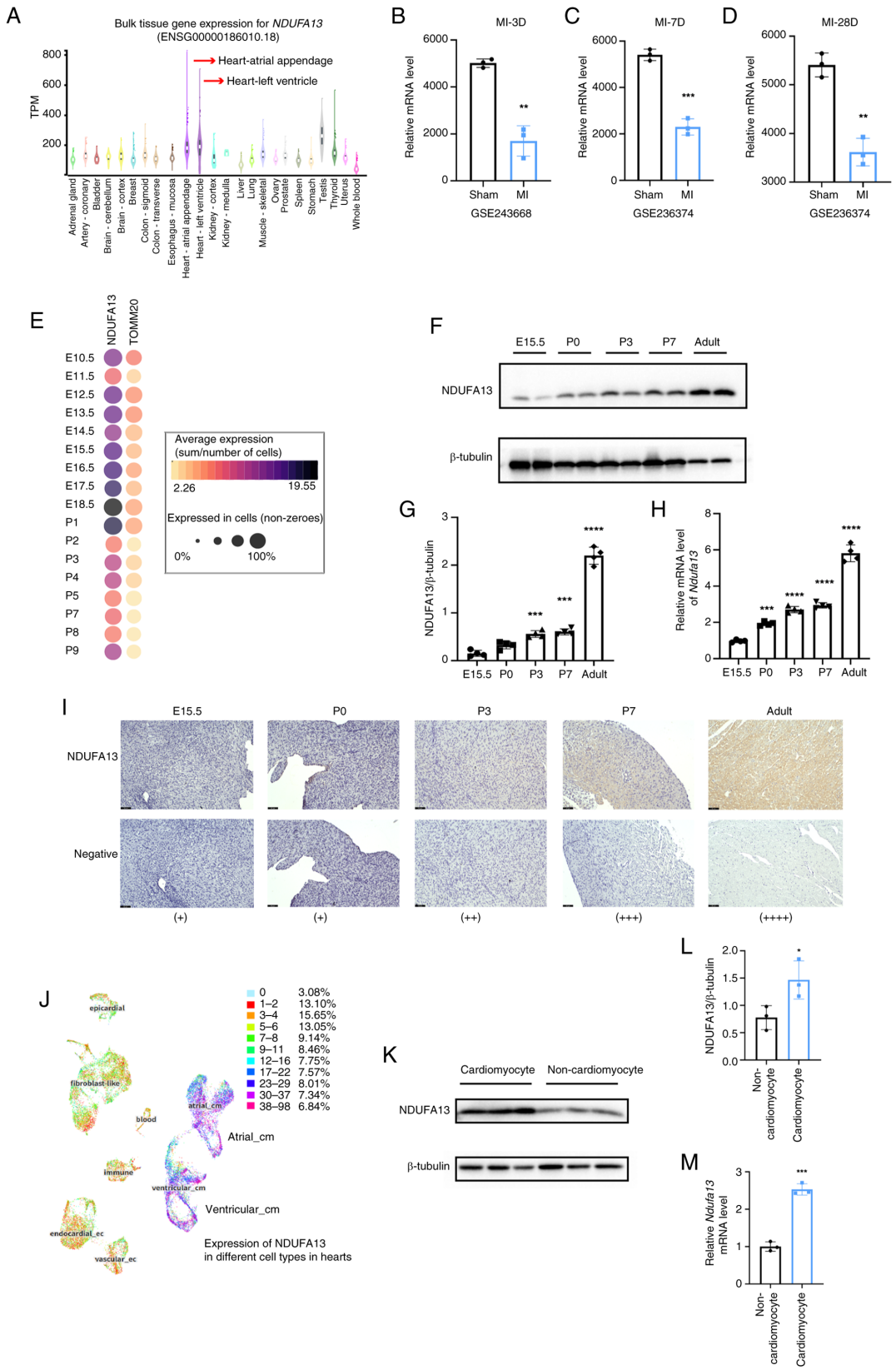

Figure 1. Expression levels of NDUFA13 in different developmental stages of mice. (A) Expression levels of NDUFA13 in various tissues from The Genotype-Tissue Expression database. Expression levels of NDUFA13 at day (B) 3, (C) 7 and (D) 28 after MI compared with that of sham mice, from GEO database. (E) Expression levels of NDUFA13 and TOMM20 (a mitochondrial marker protein) in different embryonic and neonatal period from a database (F) Western blot of NDUFA13 protein expression and (G) quantification normalized to β-tubulin in mice at stage E15.5, 0, 3 and 7 days after birth, and in adult mice (n=4). (H) mRNA levels of *Ndufa13* in mice at stage E15.5, 0, 3 and 7 days after birth, and in adult mice (n=4). (I) Immunohistochemical staining of NDUFA13 in hearts at stage E15.5, 0, 3 and 7 days after birth, and in adult mice. Scale bar, 50 μm. (J) Expression levels of NDUFA13 in different cell types in the heart from the GEO database. (K) Western blot of NDUFA13 protein expression and (L) quantification normalized to β-tubulin in cardiomyocytes and non-cardiomyocytes (n=3). (M) mRNA expression levels of *Ndufa13* in cardiomyocytes and non-cardiomyocytes (n=3). The data was presented as mean ± SD. *P<0.05, **P<0.01, ***P<0.001 and ****P<0.0001 compared with sham, E15.5 or non-cardiomyocytes group. NDUFA13, NADH dehydrogenase ubiquinone I α subcomplex 13; MI, myocardial infarction; mRNA, messenger RNA; E15.5, embryonic day 15.5; cm, cardiomyocytes; ec, endothelial cells; +, positive staining.

non-cardiomyocytes from neonatal mice. Our results indicated that NDUFA13 was highly expressed in cardiomyocytes (Fig. 1J-M), Moreover, previous studies suggested potential nuclear localization of NDUFA13 (16,17), and our results confirmed that NDUFA13 expression was predominantly expressed in the mitochondria compared with the nucleus in cardiomyocytes (Fig. 2A and B). These findings establish a clear inverse relationship between NDUFA13 expression levels and cardiomyocyte proliferative potential. However, the casual effect of NDUFA13 expression in cardiomyocyte proliferation remains unknown.

Moderately decreased expression of NDUFA13 in cardiomyocytes increases cell proliferation and promotes heart regeneration. To investigate the effects of NDUFA13 downregulation on the proliferative ability of cardiomyocytes, siRNA transfection was used to knockdown NDUFA13 in primary cardiomyocytes. Since our previous study has found that complete knockout of NDUFA13 in cells would affect the stability of mitochondria and increases apoptosis (30), a concentration of 100 nM siRNA was used to conduct moderate downregulation of NDUFA13 in cardiomyocytes based on the knockout efficiency of different siRNA concentrations as previously reported (Fig. 2C-E) (25). Following 72 h after transfection, a CCK-8 assay and immunofluorescence staining with Aurora B, Ki67 and pH3 were performed to observe the proliferative capacity of cardiomyocytes (Fig. 2F-J). They were all increased when compared with the control group. Additionally, flow cytometry was employed to analyze the cell cycle stages, which revealed that NDUFA13 downregulation promoted DNA replication in cardiomyocytes (Fig. S2). Consistent with the aforementioned results, downregulation of NDUFA13 resulted in increased proliferation capacity in cardiomyocytes.

To further explore whether NDUFA13 affected cardiomyocyte proliferation and cardiac regeneration *in vivo* following myocardial injury, transgenic *Myh6*-cre^{ERT}:*Ndufa13* $^{flox/flox}$ mice were constructed. However, previous studies have reported that complete knockout of NDUFA13 leads to embryonic developmental arrest, resulting in lethality at ~E9.5 (17,30). Meanwhile, at cellular level, excessive downregulation of NDUFA13 may affect mitochondrial stability. Therefore, for *in vivo* experiments the heterozygous genetic model, *Myh6*-cre^{ERT} *Ndufa13*$^{flox/+}$ mice, was used. Newborn mice received a 3-day course of tamoxifen injections to achieve knockdown. Following validation of the induction protocol, apical resection was performed on postnatal day 3, concurrent with the last tamoxifen administration (Fig. 3A and B).

Following surgery, key indicators were assessed at postoperative days 3, 7 and 21. For the early time points (days 3 and 7), proliferative capacity was evaluated using immunofluorescent staining of three proliferation markers: Ki67, Aurora B and pH3 (Fig. 3C-N); the positive staining of which served as quantitative measures of cardiomyocyte proliferation. Compared with the control group (*Myh6*-cre^{ERT}:*Ndufa13* $^{+/+}$), the number of cells positive for Ki67, Aurora B and pH3 in the NDUFA13-downregulated group were increased, which demonstrated an increased proliferation rate of cardiomyocytes. At 21 days post-surgery, cardiac function was assessed in both groups using echocardiography to measure ejection fraction and fractional shortening. The NDUFA13-downregulated group exhibited significantly improved cardiac function compared with that of the control group (Fig. 4A, C and D). Masson's trichrome staining demonstrated increased tissue regeneration, with control mice displaying significantly increased collagen deposition at the resection margin (Fig. 4B and E). These findings collectively demonstrated that moderate NDUFA13 downregulation promotes cardiomyocyte proliferation and facilitates cardiac repair following injury.

Downregulation of NDUFA13 is accompanied by alterations of the metabolic environment. The alteration of cardiomyocyte energy metabolism after birth is accompanied by the decrease in proliferation ability. The dominant metabolic pathway for energy production transitions from glycolysis in embryos and newborns to oxidative phosphorylation and fatty acid oxidation during maturation (19). As NDUFA13 is a part of mitochondrial complex I, it was investigated whether downregulation of NDUFA13 may influence the metabolic environment in neonatal cardiomyocytes. First, both *in vitro* and *in vivo* models were examined and found that key glycolytic enzymes, including *Pfkfb3*, hexokinase 2 (*Hk2*) and pyruvate kinase muscle isozyme M2 (*Pkm2*), were upregulated following NDUFA13 downregulation (Fig. 4F and H). By contrast, the expression levels of oxidative phosphorylation-related genes remained relatively unchanged (Fig. 4G and I), such as *Sdha*, *Cox15* and *Atp5f1a*. The expression levels of lactate dehydrogenase increased in NDUFA13-downregulated heart tissues (Fig. 4J and K). To corroborate these findings, 2-NBDG uptake assays and resident glucose measurements were performed in primary cardiomyocytes. As the results showed (Fig. 4L and M) that 2-NBDG uptake was increased, while residual glucose in the cell supernatant was reduced in the NDUFA13-downregulated group. The increased levels of glycolysis was further validated in NDUFA13-downregulated cells by assessing mitochondrial respiratory function and the glycolytic rate via and OCR and ECAR assays, respectively (Fig. 5A-F). The OCR assay demonstrated no significant differences in mitochondrial related ATP production and maximal respiration between control and NDUFA13-downregulated cells, which suggested moderate downregulation of NDUFA13 does not impair the function of mitochondria. Following the addition of rotenone and antimycin, the non-mitochondrial respiration differed between the treatment and control groups significantly. Consistently, the ECAR assay demonstrated that glycolysis and glycolytic capacity were significantly increased in NDUFA13-downregulated cells compared with that of the control group. In conclusion, moderate downregulation of NDUFA13 in cardiomyocytes could preserve the function of mitochondria, and also increase glycolysis metabolism.

Increased levels of glycolysis in cardiomyocytes are associated with increased the expression of c-Myc. c-Myc is a transcription factor (37), which serves a key role in tumor regulation (38,39). Previous studies have reported that c-Myc may increase glucose transporter expression and upregulate key enzymes in the glycolytic pathway to regulate tumor cell metabolism (40,41). Therefore, it was considered that increased levels of glycolysis may also influence the expression levels of c-Myc via a feedback loop, and expression level of c-Myc

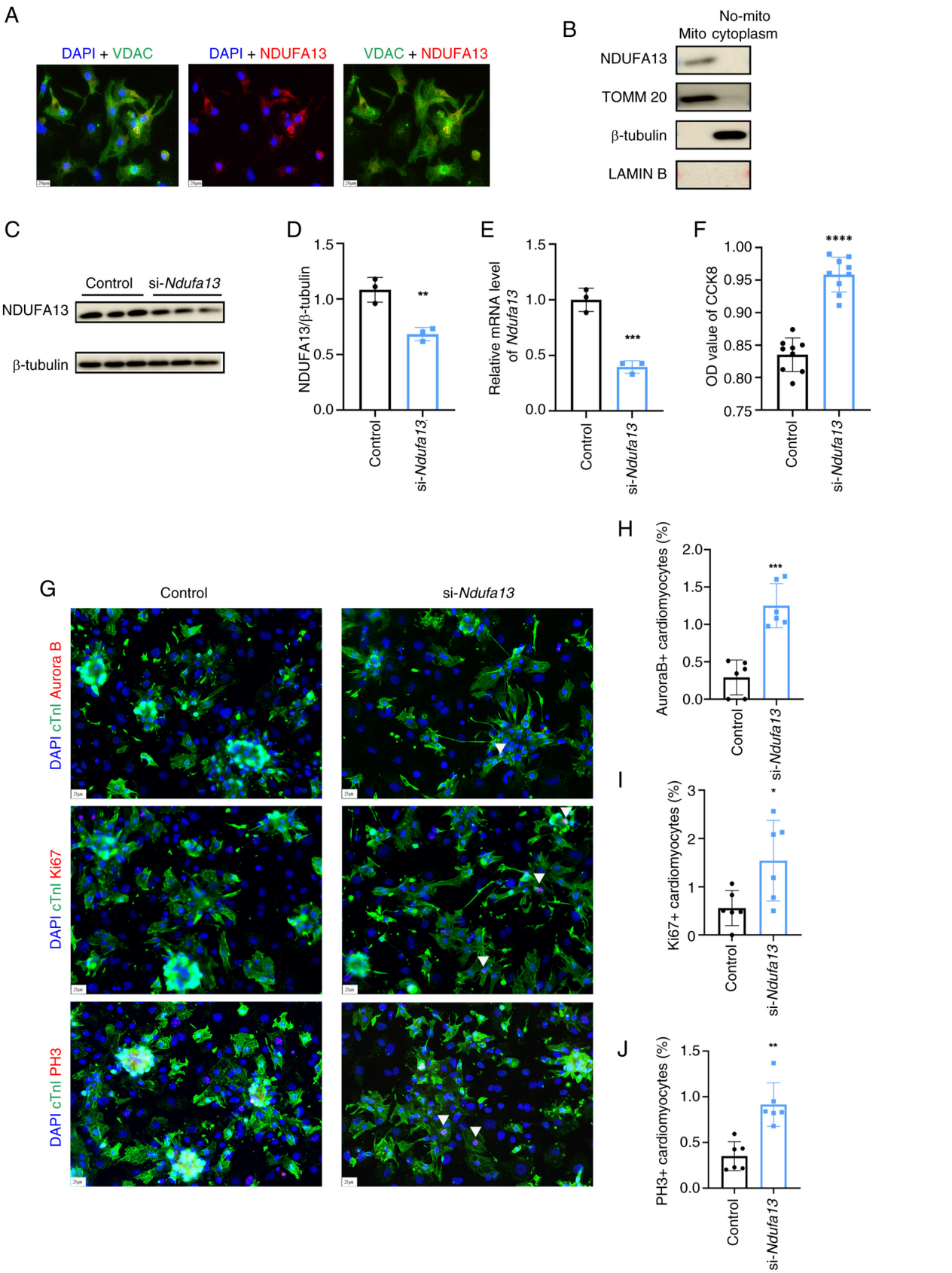

Figure 2. Moderate downregulation of NDUFA13 promotes primary cardiomyocytes proliferation. (A) Immunofluorescence and (B) western blot of NDUFA13 in primary cardiomyocytes. TOMM20, β-tubulin, and LAMIN B served as internal references for mitochondria, cytoplasm, and nucleus, respectively. Scale bar, 20 μm. (C) Western blot of NDUFA13 expression and (D) quantification normalized to β-tubulin following si-RNA transfection in primary cardiomyocytes (n=3). (E) mRNA expression levels of *Ndufa13* following si-RNA transfection in primary cardiomyocytes (n=3). (F) The OD values of the CCK8 assay of si-Ndufa13 and control cells (n=9). (G-J) Co-immunostaining of the proliferation markers Aurora B, Ki67 and pH3 (red), DAPI (blue) and cardiomyocyte marker cTnI (green) in cultured primary cardiomyocytes (n=6). The white arrows indicate positive results for the proliferation marker. Scale bar, 25 μm. The data was presented as mean ± SD. *P<0.05, **P<0.01, ***P<0.001, ****P<0.0001 compared with control group. NDUFA13, NADH dehydrogenase ubiquinone I α subcomplex 13; mRNA, messenger RNA; si-RNA, small interfering RNA; OD, optical density; pH3, phosphohistone H3; cTnI, cardiac troponin I.

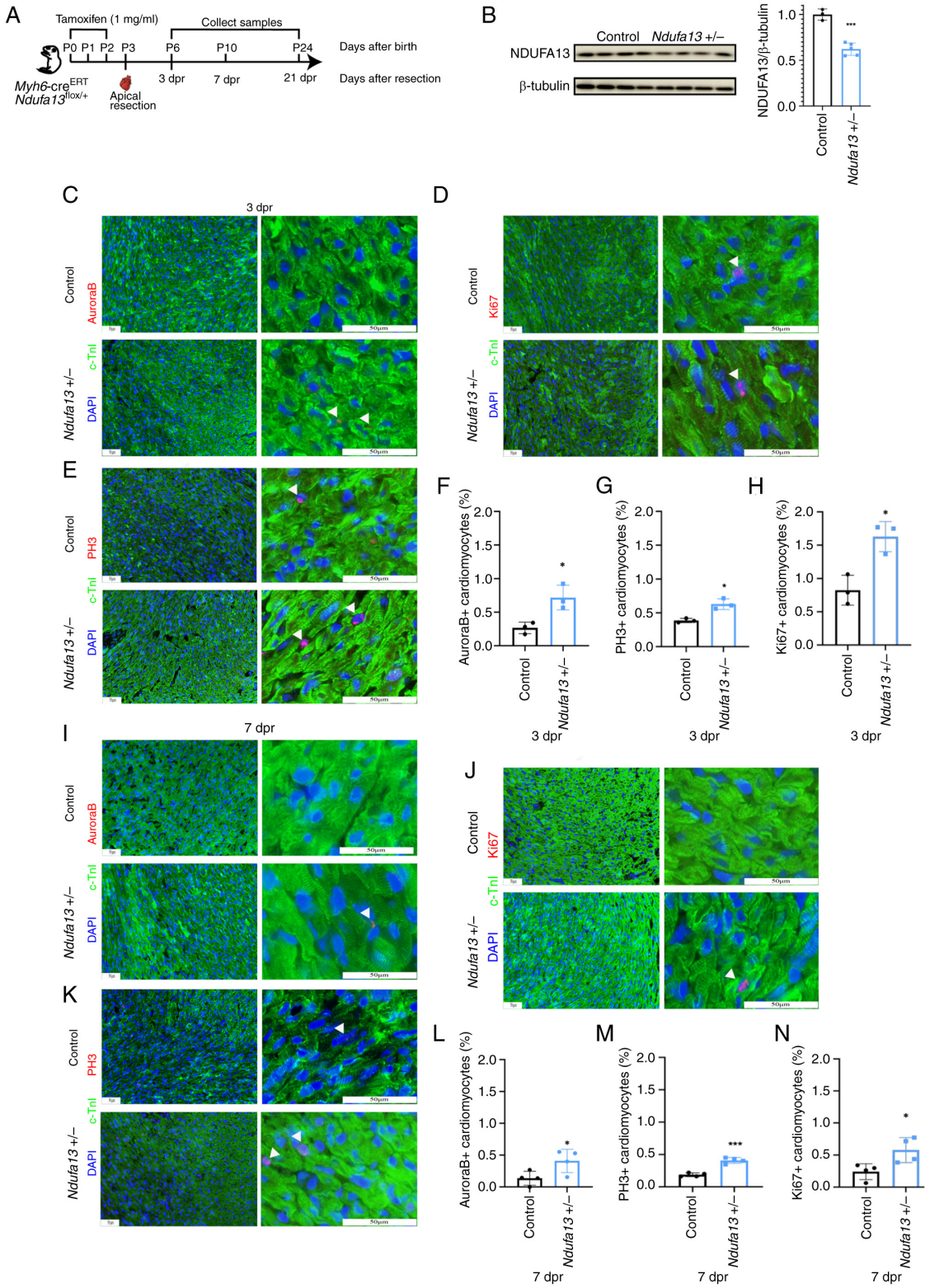

Figure 3. Moderate downregulation of NDUFA13 stimulates cardiomyocytes proliferation and heart regeneration *in vivo*. (A) Schematic diagram of the *in vivo* surgical procedure. (B) Western blot of NDUFA13 expression and quantification normalized to β-tubulin in the control and NDUFA13-downregulated models after tamoxifen injection for 3 days (control, n=3; *Ndufa13*$^{+/-}$, n=5). (C and F) Co-immunostaining and quantification of the proliferation marker Aurora B (red), DAPI (blue) and cardiomyocyte marker cTnI (green) in hearts from control and NDUFA13-downregulated mice at 3 dpr (n=3). (D and H) Co-immunostaining and quantification of the proliferation marker Ki67 (red), DAPI (blue) and cardiomyocyte marker cTnI (green) in hearts from control and NDUFA13-downregulated mice at 3 dpr (n=3). (E and G) Co-immunostaining and quantification of the proliferation marker pH3 (red), DAPI (blue) and cardiomyocyte marker cTnI (green) in hearts from control and NDUFA13-downregulated mice at 3 dpr (n=3). (I and L) Co-immunostaining and quantification of the proliferation marker Aurora B (red), DAPI (blue) and cardiomyocyte marker cTnI (green) in hearts from control and NDUFA13-downregulated mice at 7 dpr (n=4). (J and N) Co-immunostaining and quantification of the proliferation marker Ki67 (red), DAPI (blue) and cardiomyocyte marker cTnI (green) in hearts from control and NDUFA13-downregulated mice at 7 dpr (n=4). (K and M) Co-immunostaining and quantification of the proliferation marker pH3 (red), DAPI (blue) and cardiomyocyte marker cTnI (green) in hearts from control and NDUFA13-downregulated mice at 7 dpr (n=4). The white arrows indicate positive results for the proliferation marker. Scale bar, 25 μm. The data was presented as mean ± SD. *P<0.05 and ***P<0.001 compared with control group. NDUFA13, NADH dehydrogenase ubiquinone I α subcomplex 13; pH3, phosphohistone H3; cTnI, cardiac troponin I; dpr, days post resection.

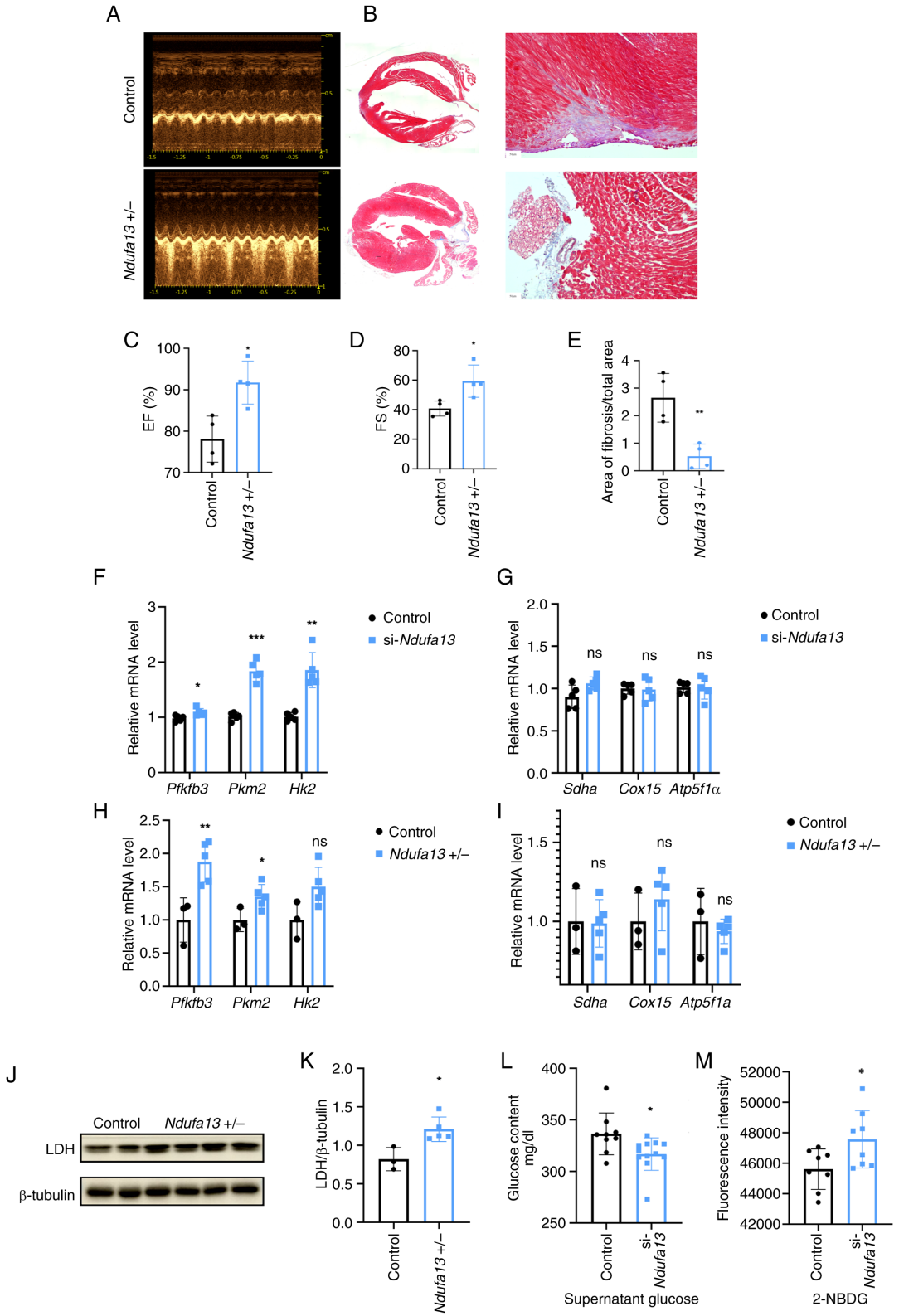

Figure 4. Moderate downregulation of NDUFA13 maintains the function of mi tochondria and increases the level of glycolysis. (A) Representative echocardiography images and analysis of the (C) EF and (D) FS after apical resection injury in control and *Ndufa13*$^{+/-}$ mice at 21 dpr (n=4). (B) Masson's trichrome staining of the hearts at 21 dpr and (E) quantification of the scar area (n=4). Scale bar, 50 μm. (F) mRNA levels of genes related to glycolysis in control and si-*Ndufa13* group (n=5). (G) mRNA levels of genes related to oxidative phosphorylation in control and si-*Ndufa13* group (n=5). (H) mRNA levels of genes related to glycolysis in control and *Ndufa13*$^{+/-}$ group (control mice, n=3; *Ndufa13*$^{+/-}$ mice, n=5). (I) mRNA levels of genes related to oxidative phosphorylation in control and *Ndufa13*$^{+/-}$ group (control mice, n=3; *Ndufa13*$^{+/-}$ mice, n=5). (J) Western blot of LDH expression levels and (K) quantification normalized to β-tubulin in control and *Ndufa13*$^{+/-}$ mice (control, n=3; *Ndufa13*$^{+/-}$, n=3). (L) The residual supernatant glucose content after 24 h culture between the two groups were compared (control, n=9; si-*Ndufa13*, n=12). (M) The fluorescence intensity of 2-NBDG after adding it to culture medium for 1 h (both groups, n=8). The data was presented as mean ± SD. *P<0.05, **P<0.01 and ***P<0.001 compared with control. NDUFA13, NADH dehydrogenase ubiquinone I α subcomplex 13; EF, ejection fraction; FS, fraction shortening; dpr, days post resection; ns, not significant; LDH, lactate dehydrogenase; Pfkfb3, 6-phosphofructo-2-kinase/fructose-2,6-bisphosphatase 3; Hk2, hexokinase 2; Pkm2, pyruvate kinase muscle isozyme M2; Sdha, succinate dehydrogenase complex flavoprotein subunit A; Cox15, cytochrome c oxidase assembly homolog 15; si-, small interfering.

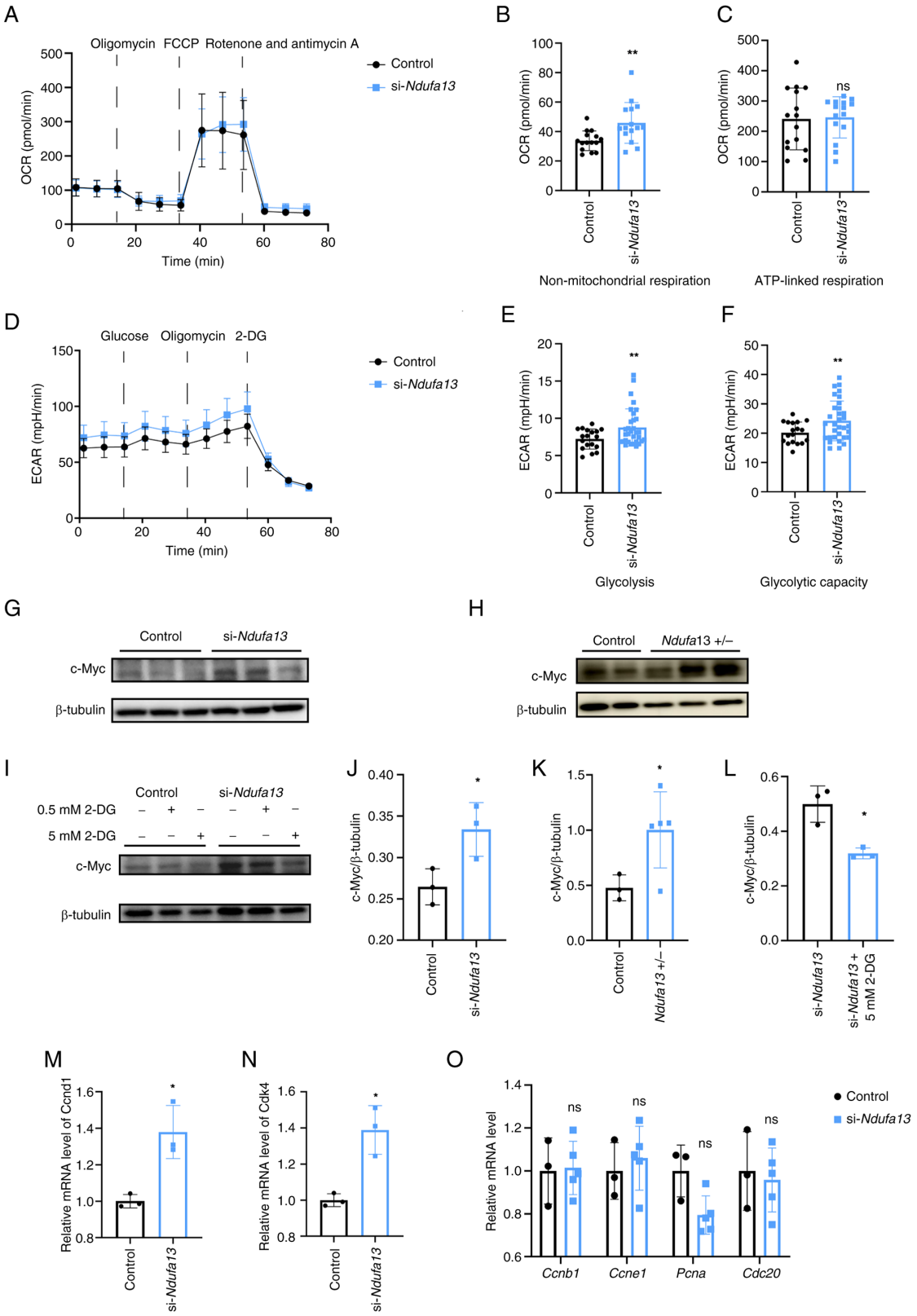

Figure 5. Increased glycolysis levels associated with increased c-Myc and *Ccnd1* expression levels. (A) The OCR of mitochondria in control and *Ndufa13*-downregulated groups. Drugs were added as following order: Oligomycin, FCCP and rotenone and antimycin A, and the (B) non-mitochondrial respiration and (C) ATP-linked respiration rates between the two groups were compared (n=15). (D) The ECAR of mitochondria in control and *Ndufa13*-downregulated groups. The drugs were added as following order: Glucose, oligomycin and 2-DG, and the (E) levels of glycolysis and (F) glycolytic capacity between the two groups were compared (control, n=18; si-*Ndufa13*, n=32). (G) Western blot of c-Myc expression and (J) quantification normalized to β-tubulin in *Ndufa13*-downregulated models (cells, n=5). (H) Western blot of c-Myc expression and (K) quantification normalized to β-tubulin in *Ndufa13*-downregulated models (control mice, n=3; *Ndufa13*$^{+/-}$ mice, n=5). (I) Western blot of c-Myc expression and (L) quantification normalized to β-tubulin in primary cardiomyocytes different concentrations of 2-DG were added (n=3). mRNA levels of (M) *Ccnd1* and (N) *Cdk4* in primary cardiomyocytes in control and *Ndufa13*$^{+/-}$ groups (n=3). (O) mRNA levels of other cell cycle related genes in primary cardiomyocytes in control and *Ndufa13*$^{+/-}$ groups (control, n=3; *Ndufa13*$^{+/-}$, n=5). The data was presented as mean ± SD. *P<0.05 and **P<0.01 compared with control. NDUFA13, NADH dehydrogenase ubiquinone I α subcomplex 13; OCR, oxygen consumption rate; ECAR, extracellular acidification rate; ns, not significant; 2-DG, 2-deoxy-glucose; Ccnb1, Cyclin B1; Ccnd1, cyclin D1; Pcna, proliferating cell nuclear antigen; Cdc20, cell division cycle 20; si-, small interfering.

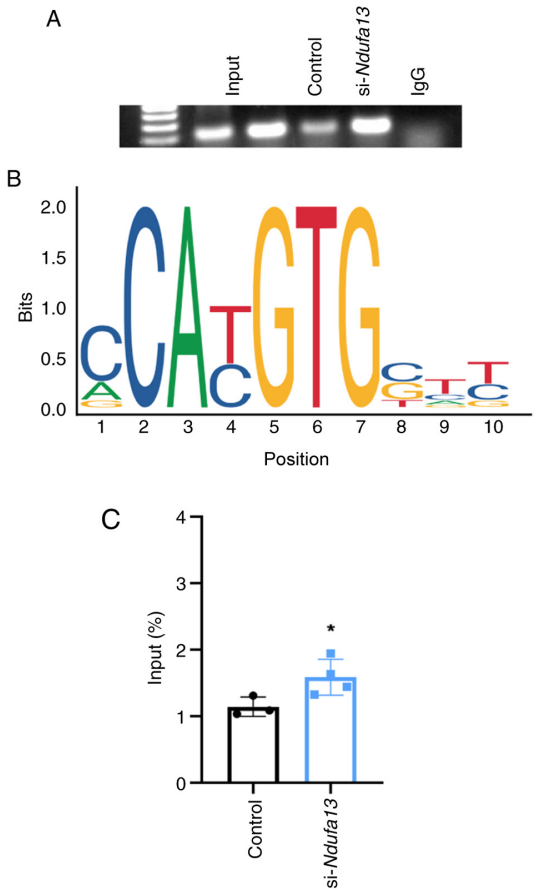

Figure 6. c-Myc binds to *Ccnd1* and stimulates the cell cycle. (A) PCR of control input, si-*Ndufa13* input, control, si-*Ndufa13* and IgG group following ChIP. (B) Forecast graph from the JASPAR database. (C) The enrichment of target regions was calculated and presented as the percentage of input DNA (Input %) in the control and si-*Ndufa13* groups (control, n=3; *Ndufa13*$^{+/-}$, n=4). The data was presented as mean ± SD. *P<0.05 compared with control. NDUFA13, NADH dehydrogenase ubiquinone I α subcomplex 13; si-small interfering.

in control and NDUFA13-downregulated primary cardiomyocytes were assessed. The expression levels of c-Myc were increased in NDUFA13-downregulated cells, which suggested that c-Myc may be associated with glycolysis or cardiomyocyte proliferation (Fig. 5G, H, J and K). To further investigate the causal relationship between c-Myc and glycolysis, 2-DG, a well-characterized glycolytic inhibitor, was utilized. The addition of 2-DG to primary cardiomyocytes resulted in decreased expression levels of c-Myc in both groups, and was notably decreased in NDUFA13-downregulated cells (Fig. 5I and L). Therefore, a glycolytic metabolic environment was associated with increases c-Myc expression.

Given the role of cell cycle regulation in proliferation, key cyclins and CDKs were analyzed representing all major cell cycle phases (G_1, S, G_2 and M) were analyzed. Expression was assessed at the transcriptional level, including markers such as cyclin B1 (*Ccnb1*), *Ccnd1*, cyclin E1 (*Ccne1*), *Cdc20*, *Cdk4*and proliferating cell nuclear antigen (42,43). Among these, *Ccnd1* was significantly increased in NDUFA13-downregulated cells (Fig. 5M-O).

c-Myc binds to gene Ccnd1 and stimulates the cell cycle. The downregulation of NDUFA13 in cardiomyocytes was associated with increased expression levels of the cell cycle gene *Ccnd1* and related kinase gene *Cdk4*. As c-Myc is a transcription factor, it was investigated whether c-Myc activated *Ccnd1* transcription via direct promoter binding (Fig. 6). The UCSC and JASPAR databases were used to predict potential binding and identify binding regions (Fig. 6B). Based on the predication results, corresponding primers were designed and validated using a ChIP assay. It was demonstrated that c-Myc binds to the promotor region of *Ccnd1* and promotes its expression (Fig. 6A and C).

In summary, moderate downregulation of NDUFA13 promoted cardiomyocyte proliferation and heart regeneration in neonatal mice after injury. In addition to preserving mitochondrial function, downregulation of NDUFA13 increased glycolysis of cardiomyocytes, which was associated with increased expression of c-Myc and cell cycle genes (Fig. 7).

Discussion

Heart failure remains a major global health challenge. Recent discoveries of cardiac regeneration in zebrafish and neonatal mammals, particularly mice (23,44,45), have indicated the potential of myocardial proliferation and heart regeneration. Multiple molecular targets have now been identified that either enhance or suppress cardiomyocyte proliferation, representing a significant advancement in cardiovascular research (46,47).

Central to this research is NDUFA13, a constituent subunit of mitochondrial complex I. NDUFA13 was originally identified as a gene found in tumor cells via tretinoin/interferon induction, which regulated apoptosis (16,48). Subsequent studies have revealed significant downregulation of NDUFA13 expression across multiple tumor types such as hepatocellular carcinoma and breast carcinoma (49,50). In cancer biology, NDUFA13 has been shown to regulate cell cycle progression, proliferation and apoptosis through downstream effectors, while also influencing tumor cell motility and migration via adhesion-related proteins (18). These findings demonstrate the key role of NDUFA13 in controlling cellular proliferation in malignant cells. In cardiomyocyte cell lines under hyperglycemic conditions, NDUFA13 downregulation was found to promote proliferation *in vitro* (41). However, its potential role in regulating cardiomyocyte proliferation and cardiac regeneration *in vivo* remains to be fully elucidated.

The regenerative ability of the mammalian heart is maintained only for a fairly short period of time after birth. Newborn mice have the ability to completely heal after myocardial injury, but this ability declines rapidly after 7 days (51,52). In order to explore whether NDUFA13 is related to the loss of proliferative capacity, embryonic, neonatal and adult mouse hearts were isolated to analyze the expression levels of NDUFA13. With increased age and the decrease of proliferative ability, the expression levels of NDUFA13 in heart tissues also gradually increased, particularly in adulthood. Therefore, it was considered that NDUFA13 expression may be associated with changes in cardiomyocyte proliferation.

To investigate the functional relationship between NDUFA13 expression and myocardial proliferation, loss-of-function approaches were employed. In primary cardiomyocytes, moderate downregulation of NDUFA13 significantly increased cellular proliferation, as evidenced

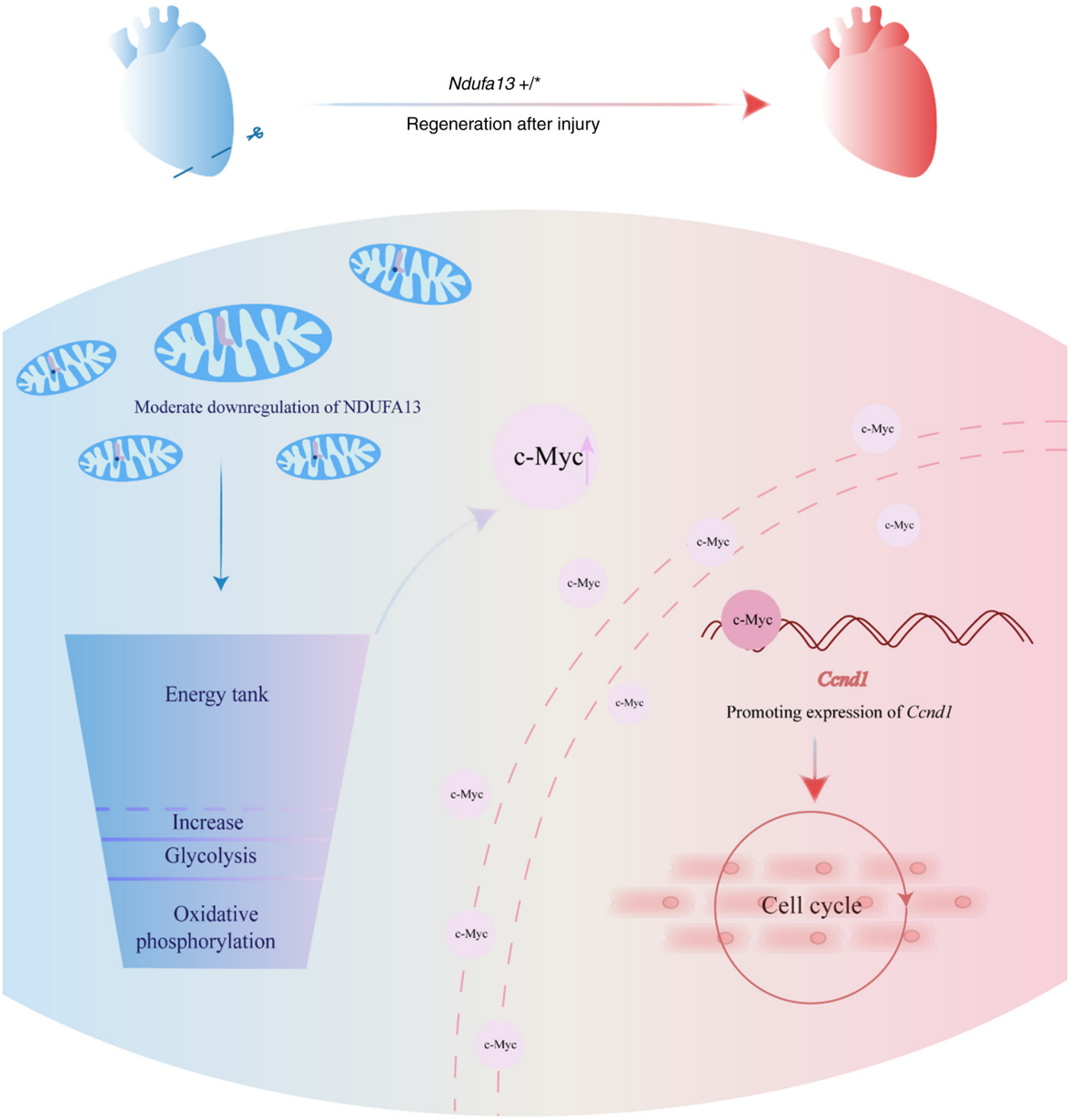

Figure 7. Schematic of the mechanism. Moderate downregulation of NDUFA13 promotes cardiomyocyte proliferation and enhances cardiac repair following injury by upregulating glycolytic flux, which was associated with elevated c-Myc expression levels. c-Myc induced transcription of *Ccnd1*, thereby accelerating cardiomyocyte proliferation. NDUFA13, NADH dehydrogenase ubiquinone I α subcomplex 13; Ccnd1, cyclin D1.

by increased cell numbers, upregulated cell cycle genes and elevated expression of proliferation markers, which suggested an inverse association between NDUFA13 expression levels and cardiomyocyte proliferative capacity. To the best of our knowledge, the present *in vivo* study demonstrated for the first time that moderate NDUFA13 downregulation, using the heterozygous knockdown of *Ndufa13* by mouse genetic model *Myh6*-cre^{ERT}:*Ndufa13*$^{flox/+}$, enhanced cardiomyocyte proliferation and promoted cardiac regeneration following apical resection. This intervention preserved cardiac function while reducing fibrotic remodeling, revealing a conserved regulatory role of NDUFA13 in cardiomyocyte proliferation.

To further elucidate how NDUFA13 regulates cardiomyocyte proliferation, its potential metabolic mechanisms were investigated. A high proliferative capacity and glycolytic metabolism characterize embryonic cardiomyocytes, whereas postnatal cardiomyocytes progressively lose their ability to proliferate and transition toward mitochondrial-dependent metabolism (23). The present results showed that NDUFA13 could regulate cardiomyocyte metabolism, as its knockdown induced a metabolic shift toward increased glycolysis. Thus, cardiomyocytes reacquired a metabolic phenotype similar to that of embryonic cardiomyocytes, thereby restoring a higher potential for proliferation. Therefore, NDUFA13 may potentially serve as a key component in the postnatal shift in cardiomyocyte metabolic patterns. Mitochondria function as the powerhouse of the cell, generating ATP to provide essential energy for cellular activity and survival. While complete knockout of NDUFA13 is lethal *in vivo* (30), the present study found that partial knockdown of NDUFA13 could enhance cardiac regeneration and protect cardiac function in mice. This response in NDUFA13-downregulated cells may reflect

the delicate metabolic balance maintained by cells, which may help to minimize further damage and ensure survival.

c-Myc, an important transcriptional factor, is closely associated with cell division and glycolysis. Previous studies have reported that c-Myc may modulate glycolytic key enzymes such as HK2, thus affecting cell metabolism (53,54). Furthermore, the glycolytic environment may also positively influence the expression of c-Myc (55). Given the observed glycolytic shift in the present study, a potential connection to c-Myc was investigated. To determine whether the glycolytic environment influenced c-Myc expression or vice versa, the glycolysis inhibitor 2-DG was used. Treatment with 2-DG significantly reduced c-Myc levels in NDUFA13-downregulated cells, demonstrating that glycolytic flux positively regulates c-Myc expression. It was postulated that c-Myc may directly bind to promoter regions of proliferation-related genes, due to its known role as a transcription factor. Through bioinformatic prediction and analysis of cell cycle gene expression patterns following NDUFA13 downregulation, *Ccnd1* was identified as a candidate target. ChIP assays confirmed direct binding of c-Myc to the *Ccnd1* promoter region, which established a mechanistic link between NDUFA13-mediated metabolic changes and cell cycle regulation.

Cardiovascular diseases remain a leading cause of global mortality, and the limited regenerative capacity of cardiomyocytes severely constrains recovery from cardiac injury, underscoring the urgent need for novel therapeutic targets. The present study identified NDUFA13 as a key regulator of cardiomyocyte proliferation and cardiac regeneration in neonatal mice, whereby moderate downregulation of NDUFA13 promoted local myocardial regeneration, reduced fibrotic tissue formation and preserved cardiac function following apical resection in mice. However, the findings in the present study are currently validated only in neonatal mouse hearts. Since neonatal cardiomyocytes retain a certain proliferative capacity, this may confound the conclusions of the present to some extent. Additionally, NDUFA13 expression was knocked down by consecutive tamoxifen injections over the first 3 days post-birth, and knockdown efficiency was confirmed via western blot to demonstrate the feasibility of this approach. However, this injection window coincides with a period of active proliferation, during which the expression of the NDUFA13 itself undergoes naturally increasing changes, potentially causing a slight discrepancy between the observed knockdown efficiency and the true efficiency. Consequently, future experiments should investigate whether reducing NDUFA13 expression in adult mouse cardiomyocytes also promotes post-injury repair. This is essential to comprehensively assess the role of NDUFA13 in promoting cardiomyocyte proliferation and cardiac regeneration, and could have implications for future clinical translation. Furthermore, it was demonstrated that NDUFA13 downregulation maintains mitochondrial function while enhancing glycolysis, but the precise molecular mechanisms underlying this metabolic shift remains to be elucidated. Further avenues of research include: i) The specific pathway through which NDUFA13 modulates glycolysis; ii) potential involvement of secondary messengers; and iii) its impact on cellular energy transduction. According to the existing literature, STAT3 functions as a key downstream effector associated with NDUFA13 (16,56). The relationship between STAT3 and NDUFA13 is complex and involves direct protein-protein interactions. It has been reported that STAT3 can directly promote the expression of key glycolytic enzymes or, alternatively, function with HIF1α to form a regulatory circuit that orchestrates cellular glycolytic reprogramming (49,57-59). Therefore, it could be hypothesized that STAT3 and HIF1α also serve important roles in mediating the promotion of cardiomyocyte proliferation induced by NDUFA13 downregulation.

In terms of targeted therapy, there are currently no drugs specifically targeting NDUFA13. Despite the availability of numerous drugs targeting mitochondrial complex I, such as rotenone, piericidin A and annonacin (60-62), whether they affect NDUFA13 remains uncertain. In addition, these drugs still face certain limitations in clinical application. Determining the appropriate degree of inhibition for mitochondrial complex I remains a critical challenge. Given that adult cardiomyocytes rely on mitochondrial oxidative phosphorylation for energy production, inappropriate suppression of complex I function may lead to contractile dysfunction and ultimately trigger heart failure. Furthermore, in addition to the heart, organs such as skeletal muscle also exhibit high energy demands, such that systemic inhibition of complex I activity carries a substantial risk of inducing functional impairments across multiple tissues (63,64). Consequently, future studies could focus on designing NDUFA13-specific targeted agents. To this end, coupling such drugs with specialized delivery systems such as liposomes or nanoparticles may enable moderate and cardiomyocyte-specific downregulation of NDUFA13 expression.

In conclusion, the present findings demonstrated that moderate NDUFA13 downregulation promotes cardiomyocyte proliferation and enhances cardiac repair following injury by upregulating glycolytic flux. This metabolic reprogramming was associated with elevated c-Myc expression levels, which in turn induced the transcription of *Ccnd1*, thereby accelerating cardiomyocyte proliferation. Therefore, the present study demonstrated that NDUFA13 may serve an important role in myocardial repair therapy in future clinical applications.

Acknowledgements

The authors would like to extend sincere gratitude to Professor Wei Zhu, Professor Jinghai Chen and Professor Hengxun Hu from Department of Cardiology, the Second Affiliated Hospital, School of Medicine, Zhejiang University for their insightful suggestions and constructive comments on the research concept and experimental design, which greatly improved the quality of this work.

Funding

The present study was supported by the Medicine and Health Science and Technology Project of Zhejiang Province (grant nos. 2022KY805 and 2024KY1071).

Availability of data and materials

The data generated in the present study are included in the figures and/or table of this article.

Authors' contributions

YG conducted writing, formal analysis, data curation and contributed to conceptualization. NQ performed data curation and contributed to conceptualization. JJ, JL and BW conducted acquisition, analysis and interpretation of the data. YW substantially contributed to the conception or design of the work, drafted the work or revised it critically for important intellectual content, secured funding and supervised the study. All authors confirmed the authenticity of all raw data, read and approved the final version of the manuscript, and agreed to be accountable for all aspects of the work in ensuring that questions related to the accuracy or integrity of any part of the work are appropriately investigated and resolved.

Ethics approval and consent to participate

The animal experiments were approved by the Animal Ethics Committee of the Second Affiliated Hospital of Zhejiang University School of Medicine (Hangzhou, China; approval no. 2019-NO.033).

Patient consent for publication

Not applicable.

Competing interests

The authors declare that they have no competing interests.

References

1. Martin SS, Aday AW, Almarzooq ZI, Anderson CAM, Arora P, Avery CL, Baker-Smith CM, Barone Gibbs B, Beaton AZ, Boehme AK, *et al*: 2024 Heart disease and stroke statistics: A report of US and global data from the American heart association. Circulation 149: e347-e913, 2024.
2. Zhao D: Epidemiological features of cardiovascular disease in Asia. JACC Asia 1: 1-13, 2021.
3. Global Burden of Cardiovascular Diseases and Risks 2023 Collaborators: Global, regional, and national burden of cardiovascular diseases and risk factors in 204 countries and territories, 1990-2023. J Am Coll Cardiol 86: 2167-2243, 2025.
4. Pezhouman A, Nguyen NB, Kay M, Kanjilal B, Noshadi I and Ardehali R: Cardiac regeneration-past advancements, current challenges, and future directions. J Mol Cell Cardiol 182: 75-85, 2023.
5. Hashimoto H, Olson EN and Bassel-Duby R: Therapeutic approaches for cardiac regeneration and repair. Nat Rev Cardiol 15: 585-600, 2018.
6. Sacks CA, Jarcho JA and Curfman GD: Paradigm shifts in heart-failure therapy-a timeline. N Engl J Med 371: 989-991, 2014.
7. Bristow MR, Saxon LA, Boehmer J, Krueger S, Kass DA, De Marco T, Carson P, DiCarlo L, DeMets D, White BG, *et al*: Cardiac-resynchronization therapy with or without an implantable defibrillator in advanced chronic heart failure. N Engl J Med 350: 2140-2150, 2004.
8. Poss KD, Wilson LG and Keating MT: Heart regeneration in zebrafish. Science 298: 2188-2190, 2002.
9. Porrello ER, Mahmoud AI, Simpson E, Hill JA, Richardson JA, Olson EN and Sadek HA: Transient regenerative potential of the neonatal mouse heart. Science 331: 1078-1080, 2011.
10. Bergmann O, Bhardwaj RD, Bernard S, Zdunek S, Barnabé-Heider F, Walsh S, Zupicich J, Alkass K, Buchholz BA, Druid H, *et al*: Evidence for cardiomyocyte renewal in humans. Science 324: 98-102, 2009.
11. Beltrami AP, Urbanek K, Kajstura J, Yan SM, Finato N, Bussani R, Nadal-Ginard B, Silvestri F, Leri A, Beltrami CA and Anversa P: Evidence that human cardiac myocytes divide after myocardial infarction. N Engl J Med 344: 1750-1757, 2001.
12. Tzahor E and Poss KD: Cardiac regeneration strategies: Staying young at heart. Science 356: 1035-1039, 2017.
13. Shrestha S, McFadden MJ, Gramolini AO and Santerre JP: Proteome analysis of secretions from human monocyte-derived macrophages post-exposure to biomaterials and the effect of secretions on cardiac fibroblast fibrotic character. Acta Biomater 111: 80-90, 2020.
14. Li F, Ren W, Zhao Y, Fu Z, Ji Y, Zhu Y and Qin C: Downregulation of GRIM-19 is associated with hyperactivation of p-STAT3 in hepatocellular carcinoma. Med Oncol 29: 3046-3054, 2012.
15. Zhou T, Chao L, Rong G, Wang C, Ma R and Wang X: Down-regulation of GRIM-19 is associated with STAT3 overexpression in breast carcinomas. Hum Pathol 44: 1773-1779, 2013.
16. Angell JE, Lindner DJ, Shapiro PS, Hofmann ER and Kalvakolanu DV: Identification of GRIM-19, a novel cell death-regulatory gene induced by the interferon-beta and retinoic acid combination, using a genetic approach. J Biol Chem 275: 33416-33426, 2000.
17. Fearnley IM, Carroll J, Shannon RJ, Runswick MJ, Walker JE and Hirst J: GRIM-19, a cell death regulatory gene product, is a subunit of bovine mitochondrial NADH:ubiquinone oxidoreductase (complex I). J Biol Chem 276: 38345-38348, 2001.
18. Huang G, Lu H, Hao A, Ng DC, Ponniah S, Guo K, Lufei C, Zeng Q and Cao X: GRIM-19, a cell death regulatory protein, is essential for assembly and function of mitochondrial complex I. Mol Cell Biol 24: 8447-8456, 2004.
19. Chen X, Wu H, Liu Y, Liu L, Houser SR and Wang WE: Metabolic reprogramming: A byproduct or a driver of cardiomyocyte proliferation?. Circulation 149: 1598-1610, 2024.
20. Cai D, Liu C, Li H, Wang C, Bai L, Feng J, Hu M, Wang H, Song S, Xie Y, *et al*: Foxk1 and Foxk2 promote cardiomyocyte proliferation and heart regeneration. Nat Commun 16: 2877, 2025.
21. Zheng L, Chen Y and Xiong JW: Rewiring cell identity and metabolism to drive cardiomyocyte proliferation. Cell Regen 14: 40, 2025.
22. Bei Y, Zhu Y, Zhou J, Ai S, Yao J, Yin M, Hu M, Qi W, Spanos M, Li L, *et al*: Inhibition of Hmbox1 promotes cardiomyocyte survival and glucose metabolism through Gck activation in ischemia/reperfusion injury. Circulation 150: 848-866, 2024.
23. Li X, Wu F, Günther S, Looso M, Kuenne C, Zhang T, Wiesnet M, Klatt S, Zukunft S, Fleming I, *et al*: Inhibition of fatty acid oxidation enables heart regeneration in adult mice. Nature 622: 619-626, 2023.
24. National Research Council (US) Committee for the Update of the Guide for the Care and Use of Laboratory Animals: Guide for the Care and Use of Laboratory Animals. 8th edition. National Academies Press, Washington, DC, 2011.
25. Liu S, Deshmukh V, Meng F, Wang Y, Morikawa Y, Steimle JD, Li RG, Wang J and Martin JF: Microtubules sequester acetylated YAP in the cytoplasm and inhibit heart regeneration. Circulation 151: 59-75, 2025.
26. Fajardo VM, Feng I, Chen BY, Perez-Ramirez CA, Shi B, Clark P, Tian R, Lien CL, Pellegrini M, Christofk H, *et al*: GLUT1 overexpression enhances glucose metabolism and promotes neonatal heart regeneration. Sci Rep 11: 8669, 2021.
27. Livak KJ and Schmittgen TD: Analysis of relative gene expression data using real-time quantitative PCR and the 2(-Delta Delta C(T)) method. Methods 25: 402-408, 2001.
28. Huang Q, Ma J, Wu H, Zhou J, Jiang L and Fei X: PDE-5-inhibited BMSCs alleviate high glucose-induced myocardial fibrosis and cardiomyocyte apoptosis by activating the cGMP/PKG pathway. Front Biosci (Landmark Ed) 28: 155, 2023.
29. Ackers-Johnson M, Li PY, Holmes AP, O'Brien SM, Pavlovic D and Foo RS: A simplified, langendorff-free method for concomitant isolation of viable cardiac myocytes and nonmyocytes from the adult mouse heart. Circ Res 119: 909-920, 2016.
30. Hu H, Nan J, Sun Y, Zhu D, Xiao C, Wang Y, Zhu L, Wu Y, Zhao J, Wu R, *et al*: Electron leak from NDUFA13 within mitochondrial complex I attenuates ischemia-reperfusion injury via dimerized STAT3. Proc Natl Acad Sci USA 114: 11908-11913, 2017.
31. Feng W, Bais A, He H, Rios C, Jiang S, Xu J, Chang C, Kostka D and Li G: Single-cell transcriptomic analysis identifies murine heart molecular features at embryonic and neonatal stages. Nat Commun 13: 7960, 2022.
32. Lee KCY, Williams AL, Wang L, Xie G, Jia W, Fujimoto A, Gerschenson M and Shohet RV: PKM2 regulates metabolic flux and oxidative stress in the murine heart. Physiol Rep 12: e70040, 2024.

33. Yu P, Song S, Zhang X, Cui S, Wei G, Huang Z, Zeng L, Ni T and Sun A: Downregulation of apoptotic repressor AVEN exacerbates cardiac injury after myocardial infarction. Proc Natl Acad Sci USA 120: e2302482120, 2023.
34. Hao H, Liu J, Liu G, Guan D, Yang Y, Zhang X, Cao X and Liu Q: Depletion of GRIM-19 accelerates hepatocellular carcinoma invasion via inducing EMT and loss of contact inhibition. J Cell Physiol 227: 1212-1219, 2012.
35. Wang T, Yan XB, Zhao JJ, Ye J, Jiang ZF, Wu DR, Xiao WH and Liu RY: Gene associated with retinoid-interferon-induced mortality-19 suppresses growth of lung adenocarcinoma tumor in vitro and in vivo. Lung Cancer 72: 287-293, 2011.
36. Mouton AJ, Li X, Hall ME and Hall JE: Obesity, hypertension, and cardiac dysfunction: Novel roles of immunometabolism in macrophage activation and inflammation. Circ Res 126: 789-806, 2020.
37. Jakobsen ST and Siersbæk R: Transcriptional regulation by MYC: An emerging new model. Oncogene 44: 1-7, 2025.
38. Miller DM, Thomas SD, Islam A, Muench D and Sedoris K: c-Myc and cancer metabolism. Clin Cancer Res 18: 5546-5553, 2012.
39. Kato GJ and Dang CV: Function of the c-Myc oncoprotein. FASEB J 6: 3065-3072, 1992.
40. Duan R, Zhai Y, Wang Q, Zhao L, Wang Y, Yu N, Zhang J and Guo W: LINC01764 promotes colorectal cancer cells proliferation, metastasis, and 5-fluorouracil resistance by regulating glucose and glutamine metabolism via promoting c-MYC translation. MedComm (2020) 5: e70003, 2024.
41. Yang Y, Li S, Shi W, Jin G, Guo D, Li A, Wang B, Lu B and Feng S: Pterostilbene suppresses the growth of esophageal squamous cell carcinoma by inhibiting glycolysis and PKM2/STAT3/c-MYC signaling pathway. Int Immunopharmacol 142: 113247, 2024.
42. Suski JM, Braun M, Strmiska V and Sicinski P: Targeting cell-cycle machinery in cancer. Cancer Cell 39: 759-778, 2021.
43. Otto T and Sicinski P: Cell cycle proteins as promising targets in cancer therapy. Nat Rev Cancer 17: 93-115, 2017.
44. Ji X, Chen Z, Wang Q, Li B, Wei Y, Li Y, Lin J, Cheng W, Guo Y, Wu S, *et al*: Sphingolipid metabolism controls mammalian heart regeneration. Cell Metab 36: 839-856.e8, 2024.
45. Gao F, Liang T, Lu YW, Pu L, Fu X, Dong X, Hong T, Zhang F, Liu N, Zhou Y, *et al*: Reduced mitochondrial protein translation promotes cardiomyocyte proliferation and heart regeneration. Circulation 148: 1887-1906, 2023.
46. Du J, Zheng L, Gao P, Yang H, Yang WJ, Guo F, Liang R, Feng M, Wang Z, Zhang Z, *et al*: A small-molecule cocktail promotes mammalian cardiomyocyte proliferation and heart regeneration. Cell Stem Cell 29: 545-558.e13, 2022.
47. Feng J, Li Y, Li Y, Yin Q, Li H, Li J, Zhou B, Meng J, Lian H, Wu M, *et al*: Versican promotes cardiomyocyte proliferation and cardiac repair. Circulation 149: 1004-1015, 2024.
48. Hofmann ER, Boyanapalli M, Lindner DJ, Weihua X, Hassel BA, Jagus R, Gutierrez PL and Kalvakolanu DV: Thioredoxin reductase mediates cell death effects of the combination of beta interferon and retinoic acid. Mol Cell Biol 18: 6493-6504, 1998.
49. Liu Q, Wang L, Wang Z, Yang Y, Tian J, Liu G, Guan D, Cao X, Zhang Y and Hao A: GRIM-19 opposes reprogramming of glioblastoma cell metabolism via HIF1α destabilization. Carcinogenesis 34: 1728-1736, 2013.
50. Nallar SC and Kalvakolanu DV: GRIM-19: A master regulator of cytokine induced tumor suppression, metastasis and energy metabolism. Cytokine Growth Factor Rev 33: 1-18, 2017.
51. Li F, Wang X, Capasso JM and Gerdes AM: Rapid transition of cardiac myocytes from hyperplasia to hypertrophy during postnatal development. J Mol Cell Cardiol 28: 1737-1746, 1996.
52. Soonpaa MH, Kim KK, Pajak L, Franklin M and Field LJ: Cardiomyocyte DNA synthesis and binucleation during murine development. Am J Physiol 271: H2183-H2189, 1996.
53. Han X, Ren C, Lu C, Qiao P, Yang T and Yu Z: Deubiquitination of MYC by OTUB1 contributes to HK2 mediated glycolysis and breast tumorigenesis. Cell Death Differ 29: 1864-1873, 2022.
54. Yeung SJ, Pan J and Lee MH: Roles of p53, MYC and HIF-1 in regulating glycolysis-the seventh hallmark of cancer. Cell Mol Life Sci 65: 3981-3999, 2008.
55. Clementino M, Xie J, Yang P, Li Y, Lin HP, Fenske WK, Tao H, Kondo K, Yang C and Wang Z: A positive feedback loop between c-Myc upregulation, glycolytic shift, and histone acetylation enhances cancer stem cell-like property and tumorigenicity of Cr(VI)-transformed cells. Toxicol Sci 177: 71-83, 2020.
56. Alas S and Bonavida B: Rituximab inactivates signal transducer and activation of transcription 3 (STAT3) activity in B-non-Hodgkin's lymphoma through inhibition of the interleukin 10 autocrine/paracrine loop and results in down-regulation of Bcl-2 and sensitization to cytotoxic drugs. Cancer Res 61: 5137-5144, 2001.
57. Li Y, Song Z, Han Q, Zhao H, Pan Z, Lei Z and Zhang J: Targeted inhibition of STAT3 induces immunogenic cell death of hepatocellular carcinoma cells via glycolysis. Mol Oncol 16: 2861-2880, 2022.
58. Poli V and Camporeale A: STAT3-mediated metabolic reprograming in cellular transformation and implications for drug resistance. Front Oncol 5: 121, 2015.
59. Grillo M, Palmer C, Holmes N, Sang F, Larner AC, Bhosale R and Shaw PE: Stat3 oxidation-dependent regulation of gene expression impacts on developmental processes and involves cooperation with Hif-1α. PLoS One 15: e0244255, 2020.
60. Zhang W, Yang Y, Gao H, Zhang Y, Jia Z and Huang S: Inhibition of mitochondrial complex I aggravates folic acid-induced acute kidney injury. Kidney Blood Press Res 44: 1002-1013, 2019.
61. Trushin S, Nguyen T, Stojakovic A, Ostroot M, Deason JT, Chang SY, Zhang L, Macura SI, Nambara T, Lu W, *et al*: Therapeutic assessment of a novel mitochondrial complex I inhibitor in in vitro and in vivo models of Alzheimer's disease. EBioMedicine 120: 105924, 2025.
62. Al Assi A, Posty S, Lamarche F, Chebel A, Guitton J, Cottet-Rousselle C, Prudent R, Lafanechère L, Giraud S, Dallemagne P, *et al*: A novel inhibitor of the mitochondrial respiratory complex I with uncoupling properties exerts potent antitumor activity. Cell Death Dis 15: 311, 2024.
63. Yap TA, Daver N, Mahendra M, Zhang J, Kamiya-Matsuoka C, Meric-Bernstam F, Kantarjian HM, Ravandi F, Collins ME, Francesco MED, *et al*: Complex I inhibitor of oxidative phosphorylation in advanced solid tumors and acute myeloid leukemia: Phase I trials. Nat Med 29: 115-126, 2023.
64. Machado ND, Heather LC, Harris AL and Higgins GS: Targeting mitochondrial oxidative phosphorylation: Lessons, advantages, and opportunities. Br J Cancer 129: 897-899, 2023.